SIAM J. MATH. ANAL.
Vol. 24, No. 5, pp. 1215–1225, September 1993

005

SINGULARITIES OF THE X-RAY TRANSFORM AND LIMITED DATA TOMOGRAPHY IN $\mathbb{R}^2$ AND $\mathbb{R}^3$*

ERIC TODD QUINTO†

Abstract. Given a function f, the author specifies the singularities of f that are visible in a stable way from limited X-ray tomographic data. This determines which singularities of f can be stably recovered from limited data and which cannot, no matter how good the inversion algorithm. Microlocal analysis is used to determine the relationship between the singularities of a function f and those of its X-ray transform. The results are applied to determine the singularities that are visible for limited angle tomography and the interior and exterior problems. The author also suggests a practical method to use this relationship to reconstruct singularities of f from limited data Rf. The X-ray transform with sources on a curve in $\mathbb{R}^3$ is also analyzed.

Key words. X-ray transform, limited data tomography, microlocal analysis

AMS subject classifications. primary 44A12, 92C55; secondary 35S30, 58G15

1. Introduction. X-ray tomography is an important, noninvasive, practical way of finding the density of objects. In standard tomography, X-rays of the object are taken over an evenly distributed set of lines, so-called *complete tomographic data*, and well-known algorithms are used to recover a good approximation to that object [21]. Inversion is only mildly ill-conditioned (continuous of order $\frac{1}{2}$ in Sobolev norms). However, one often needs to find the density of an object but one cannot get X-ray tomographic data over an evenly spaced set of lines through the object but only some subset; one has *limited tomographic data.* Limited data tomography is important in medical imaging [21], scientific tomography [1], and industrial nondestructive evaluation [28].

In general, reconstruction from limited tomographic data is much more highly ill-posed than reconstruction from complete data [6]. As a result, inversion algorithms using limited data, generally, can create artifacts, blurring or other distortions in their reconstructions. The goal of this article is to classify what singularities can be stably reconstructed from limited data and what singularities cannot be stably reconstructed no matter how good the algorithm. To do this, we will use a precise concept of singularity: *the wavefront set,* and a precise concept of stability: *continuity in microlocal Sobolev norms.* Then we will tell which singularities the X-ray transform "sees" stably and which singularities are not stably detected from limited data. The reason we can do this is because the X-ray transform is an elliptic Fourier integral operator and, therefore, changes wavefront sets in specific ways.

We do not claim that all limited data tomography algorithms will reconstruct the "visible" singularities well. Rather, we claim that, if a singularity is not stably visible from limited data, no algorithm can reconstruct it stably. For "visible" singularities our theorem gives stability estimates of order $\frac{1}{2}$ in Sobolev norms, so one would ex-

*Received by the editors July 13, 1992; accepted for publication (in revised form) February 8, 1993.

† Department of Mathematics, Tufts University, Medford, Massachusetts 02155 (equinto@math.tufts.edu). The author was partially supported by the Emmy Noether Institute at Bar Ilan University, the Humboldt Stiftung, and National Science Foundation grants MCS 8901203 and MCS 9123862.

pect "visible" singularities to be well constructed by a "good" algorithm even in the presence of noise.

This work is a natural outgrowth of [26], which gave the general principle (3.3) we make more precise and then prove in §3–4. Palamodov stated a closely related idea in [22]. The "tangent casting" effects of [30] is an intuitive way of expressing (3.3) below. One can also understand stability of these problems using singular value decompositions [4], [14], [16], [17], [18]. Lambda tomography [5] is a well developed algorithm that finds singularities of a function from real tomographic data. Their method works quite well with interior data (Example 3.3). Ramm and Zaslavsky [29] have developed a method using Legendre transforms to reconstruct the singularities of a function from knowing the singularities of its Radon transform. They consider functions $f = \psi\chi_D$, where D is a piecewise smooth domain and ψ is smooth—functions with the jump singularities on ∂D, and they use the behavior of Rf at ∂D to find the (jump) singularities of f. Technicians currently use the sinogram, the graph of $Rf(\theta, p)$ in rectangular coordinates, to find boundaries, but this method is subjective.

In Remark 3.2, we propose a method to reconstruct singularities (classified by Sobolev wavefront set) for arbitrary functions from general limited data.

Section 2 of this article provides the definitions of singularity and microlocal Sobolev smoothness. In §3 we give the singularity result for the Radon transform in the plane, Theorem 3.1. We apply this to determining singularities of arbitrary functions from general limited data (Remark 3.2) and to show limitations inherent in the common types of limited data tomography (Examples 3.3–3.5). Reconstructions from exterior data are presented that illustrate our analysis. §4 gives analysis and results for the X-ray transform with sources on a curve in $\mathbb{R}^3$.

2. Microlocal singularities and Sobolev spaces. Our development is valid for distributions as well as functions, so first, we recall some basic definitions. $\mathcal{D}(\mathbb{R}^n)$ is the space of C^∞ functions of compact support. A distribution $f \in \mathcal{D}'(\mathbb{R}^n)$ is a continuous linear functional on $\mathcal{D}(\mathbb{R}^n)$. A distribution f has compact support if there is a compact set $K \subset \mathbb{R}^n$ such that $f(\phi) = 0$ for all functions $\phi \in \mathcal{D}(\mathbb{R}^n)$ with support disjoint from K, that is, f is zero outside of K. The set of distributions of compact support is denoted by $\mathcal{E}'(\mathbb{R}^n)$.

The wavefront set of $f \in \mathcal{D}'(\mathbb{R}^n)$ is a powerful classification of singularities because it involves not only a point x_0 at which f is not smooth, but also a *direction* in which f is not smooth at x_0. To understand this we recall some facts about the Fourier transform. When f has compact support, then f is equal to a C^∞ function almost everywhere if and only if its Fourier transform, $\mathcal{F}f$, decreases rapidly in all directions (for all $N \in \mathbb{N}$, there exists C_N such that for all $\xi \in \mathbb{R}^n$, $|\mathcal{F}f(\xi)| \leq C_N(1 + |\xi|)^{-N}$). This relates global smoothness of f to rapid decrease of its Fourier transform. A local version of this at a point $x_0 \in \mathbb{R}^n$ would be obtained by multiplying f by a smooth cut-off function, ϕ (with $\phi(x_0) \neq 0$) and seeing if this Fourier transform is rapidly decreasing in every direction. However, this localized Fourier transform $\mathcal{F}(\phi f)$ gives even more specific information—microlocal information—namely, the *directions* in which $\mathcal{F}(\phi f)$ does not decrease rapidly.

DEFINITION 2.1. Let $f \in \mathcal{D}'(\mathbb{R}^n)$ and let $x_0 \in \mathbb{R}^n$ and $\xi_0 \in \mathbb{R}^n \setminus 0$. Then we say $(x_0, \xi_0) \in \mathrm{WF}f$, the wavefront set of f, if and only if for each cut-off function at x_0, $\phi \in \mathcal{D}(\mathbb{R}^n)$ with $\phi(x_0) \neq 0$, $\mathcal{F}(\phi f)$ does not decrease rapidly in any open conic neighborhood of the ray $\{t\xi_0 | t > 0\}$.

For example, if $D \subset \mathbb{R}^n$ has smooth boundary, then $\mathrm{WF}\chi_D$ is exactly the set of normals to ∂D. One can prove this using the definition and a local coordinate change

to flatten ∂D locally. If ψ is a smooth function then $\mathrm{WF}\psi\chi_D \subset \mathrm{WF}\chi_D$, and if ψ is not zero anywhere on ∂D, then these sets are equal [11], [24, Lemma 13.3, p. 279].

As defined, $\mathrm{WF}f$ is a closed subset of $\mathbb{R}^n \times (\mathbb{R}^n \setminus 0)$ that is conic in the second variable. The Sobolev space analogue to the concept of microlocal smoothness is as follows (see [24, p. 259]).

DEFINITION 2.2. A distribution f is in the Sobolev space H^s microlocally near (x_0, ξ_0) if and only if there is a cut-off function $\phi \in \mathcal{D}(\mathbb{R}^n)$ with $\phi(x_0) \neq 0$ and function $u(\xi)$ homogeneous of degree zero and smooth on $\mathbb{R}^n \setminus 0$ and with $u(\xi_0) \neq 0$ such that $u(\xi)\mathcal{F}(\phi f)(\xi) \in L^2(\mathbb{R}^n, (1+|x|^2)^s)$.

First, one localizes near x_0 by multiplying f by ϕ and then one takes Fourier transform. Finally, one *microlocalizes* near ξ_0 by forming $u\mathcal{F}f$ and see if this is in $\mathcal{F}\big(H^s(\mathbb{R}^n)\big)$. It follows from the definition that, if $(x_0, \xi_0) \notin \mathrm{WF}f$, then for all s, f is H^s near (x_0, ξ_0).

Wavefront set and microlocal smoothness are usually defined on $T^*(\mathbb{R}^n) \setminus 0$, the cotangent space of $\mathbb{R}^n$ with its zero section removed, because such a definition can be extended invariantly to manifolds using local coordinates. For the manifold $[0, 2\pi] \times \mathbb{R}$, choosing a function $\phi(\theta, p)$ with sufficiently small support allows one to use θ and p as local coordinates. We will use these conventions.

3. The X-ray transform in the plane. In $\mathbb{R}^2$ the microlocal analysis of the X-ray transform is easier to describe if one uses parallel-beam geometry rather than fan-beam geometry. By rebinning—a coordinate change—the results are the same as for fan-beam data for functions supported inside the circle of sources. First, let $\cdot$ denote the standard inner product on $\mathbb{R}^2$; let $|\ |$ be the induced norm. Let $\theta \in [0, 2\pi]$, and let $p \in \mathbb{R}$. Let $\overline{\theta} = (\cos\theta, \sin\theta)$ and $\theta^\perp = (-\sin\theta, \cos\theta)$. Now let $\ell(\theta, p) = \{x \in \mathbb{R}^2 | x \cdot \overline{\theta} = p\}$, the line with normal vector $\overline{\theta}$ and directed distance p from the origin. The points (θ, p) and $(\theta + \pi, -p)$ parameterize the same line $\ell(\theta, p)$. Let ds be arc length, the measure on $\ell(\theta, p)$ induced from Lebesgue measure on $\mathbb{R}^2$. The classical X-ray transform in the plane is defined for an integrable function f on $\mathbb{R}^2$ by

$$Rf(\theta, p) = \int_{y \in \ell(\theta, p)} f(y) ds. \tag{3.1}$$

$Rf(\theta, p)$ is the integral of f over the line $\ell(\theta, p)$.

In order to describe the main theorem, we will consider wavefront sets as subsets of cotangent spaces. To this end, let $x_0 \in \mathbb{R}^2$. If $y = (y_1, y_2) \in \mathbb{R}^2$, then we let $y\mathbf{dx} = y_1\mathbf{dx}_1 + y_2\mathbf{dx}_2$ be the cotangent vector corresponding to y in $T^*_{x_0}\mathbb{R}^2$. Now let $(\theta_0, p_0) \in [0, 2\pi] \times \mathbb{R}$. Here we will identify $[0, 2\pi]$ with the unit circle by equating zero with 2π. Then for $(\theta, p) \in [0, 2\pi] \times \mathbb{R}$, we let $\mathbf{d\theta}$ and $\mathbf{dp}$ be the standard basis of $T^*_{(\theta,p)}([0, 2\pi] \times \mathbb{R})$. The theorem follows.

THEOREM 3.1. *Let $f \in \mathcal{E}'(\mathbb{R}^2)$. If $(x; \xi) \in T^*(\mathbb{R}^n) \setminus O$ is not conormal to $\ell(\theta_0, p_0)$, then wavefront set of f at $(x; \xi)$ does not contribute to* $\mathrm{WF}Rf$ *above (θ_0, p_0). Let $x_0 \in \ell(\theta_0, p_0)$ and let $\eta_0 = \mathbf{dp} - (x_0 \cdot \theta_0^\perp)\mathbf{d\theta}$. Let $a \neq 0$. The correspondence between* $\mathrm{WF}f$ *and* $\mathrm{WF}Rf$ *is*:

$$(x_0; a\overline{\theta}_0\mathbf{dx}) \in \mathrm{WF}f \quad \textit{if and only if } (\theta_0, p_0; a\eta_0) \in \mathrm{WF}Rf. \tag{3.2}$$

Given $(\theta_0, p_0; a\eta_0)$, $(x_0; a\overline{\theta}_0\mathbf{dx})$ is uniquely determined by (3.2). *Moreover, $f \in H^s$ is microlocally near $(x_0; a\overline{\theta}_0\mathbf{dx})$ if and only if $Rf \in H^{s+1/2}$ is microlocally near $(\theta_0, p_0; a\eta_0)$.*

Theorem 3.1 provides an exact correspondence between singularities of f and those of Rf. Moreover, it states that the singularities of Rf that are detected are

of Sobolev order $\frac{1}{2}$ smoother than the corresponding singularities of f. For typical singularities of f (jump singularities in $H^{1/2-\epsilon}$) one can realistically expect the corresponding singularities of Rf not to be masked by noise. Reconstructions given in Figs. 1 and 2 will corroborate this.

The theorem has this simple corollary:

(3.3)
The X-ray transform data Rf for (θ, p) arbitrarily near (θ_0, p_0) detects singularities of f perpendicular to the line $\ell(\theta_0, p_0)$ but not in other directions.

This follows because of the correspondence (3.2): $Rf(\theta, p)$ is smooth near (θ_0, p_0) (no wavefront set near this point) if and only if there is no wavefront set of f at points on $\ell(\theta_0, p_0)$ conormal to the line.

As an example, let D be a compact set with smooth boundary and let $f = \psi\chi_D$, where ψ is a smooth function that is not zero anywhere on ∂D. Then, by (3.3), $Rf(\theta, p)$ is smooth near (θ_0, p_0) if and only if $\ell(\theta_0, p_0)$ is not tangent to ∂D. If ∂D is not smooth then more wavefront directions will appear at points where ∂D is not smooth. Remark 3.2 gives a more general observation with practical implications.

Remark 3.2. The correspondence (3.2) gives a way to find WFf from knowing WFRf. Given $(\theta_0, p_0; a\eta_0) \in \mathrm{WF}Rf$, the rule (3.2) determines $(x_0; a\overline{\theta}_0 \mathbf{d}\boldsymbol{x})$ uniquely. This method to find singularities of f is easiest to describe in the case f is C^1 except for jump singularities on a collection, E, of C^1 curves. In this case, almost all singularities of f are in $H^{1/2-\epsilon}$ (so corresponding singularities of Rf are in $H^{1-\epsilon}$) for $\epsilon > 0$ but not for $\epsilon = 0$. One can take a local (discrete) Fourier transform of Rf in (θ, p) and find the directions in which the localized transform is not in $\mathcal{F}H^1$. Perhaps this can be efficiently done just by calculating local fast Fourier transforms and looking for directions in which they do not decrease quickly. Then the rule (3.2) gives the covectors $(x_0; a\overline{\theta}_0 \mathbf{d}\boldsymbol{x})$ at which f is not $H^{1/2}$. These covectors specify the jump singularities of f, that is the location of E (and $\overline{\theta}_0$ even gives the normal to E at x_0). This method also filters out noise that is H^1 or smoother.

This method can be used for limited data problems: the method is local in the strong sense that singularities of Rf at (θ_0, p_0) (and therefore the corresponding singularities of f on $\ell(\theta_0, p_0)$) are determined by data $Rf(\theta, p)$ for (θ, p) near (θ_0, p_0). This method is being pursued.

Proof of Theorem 3.1. The microlocal correspondence between WFf and WFRf is in the literature (e.g., [8], [25]), but since it is especially straightforward in this case, it will be given here. First, note that the Schwartz kernel of the operator R is the distribution on $\mathbb{R}^2 \times \big([0, 2\pi] \times \mathbb{R}\big)$ that is integration with respect to the weight $dxd\theta$ over the set $Z = \{(x, \theta, p) | x \cdot \overline{\theta} = p\}$. This is a special type of distribution and in [10] it is shown to be a Fourier integral distribution associated with the Lagrangian manifold $\Gamma = N^*Z \setminus 0$ where N^*Z is the conormal bundle of Z in $T^*\big(\mathbb{R}^2 \times ([0, 2\pi] \times \mathbb{R})\big)$. As shown in [8] (see also [25] for details), because the measure of integration $dxd\theta$ is nowhere zero and the projection from Γ to $T^*([0, 2\pi] \times \mathbb{R}) \setminus 0$ is a injective immersion, R is elliptic with elliptic inverse that composes well with R. To understand what R does to wavefront sets, one must calculate the set Γ. Z is defined by the equation $x \cdot \overline{\theta} - p = 0$ and so its differential, $\overline{\theta}\mathbf{d}\boldsymbol{x} + x \cdot \theta^{\perp}\mathbf{d}\boldsymbol{\theta} - \mathbf{d}\boldsymbol{p}$, is a basis of N^*Z at each point. Therefore,

$$\Gamma = \big\{\big(x, \theta, p; a(\overline{\theta}\mathbf{d}\boldsymbol{x} + x \cdot \theta^{\perp}\mathbf{d}\boldsymbol{\theta} - \mathbf{d}\boldsymbol{p})\big) \big| (x, \theta, p) \in Z,\ a \neq 0\big\}. \tag{3.4}$$

By the calculus of elliptic Fourier integral operators, there is a simple correspondence between WFf and WFRf: $(x; \xi) \in \mathrm{WF}f$ if and only if there is a $(\theta, p; \eta) \in \mathrm{WF}Rf$

with $(x,\theta,p;\xi,-\eta)\in\Gamma$ [31]. Using (3.4) we see this correspondence is exactly (3.2). Furthermore this correspondence coming from (3.4) shows that if $(x;\xi)$ is not conormal to $\ell(\theta_0,p_0)$, then wavefront set of f at $(x;\xi)$ does not contribute to WFRf above (θ_0,p_0). To see that (3.2) uniquely determines $(x_0;\overline{\theta}_0\mathbf{d}\boldsymbol{x})$, first note that a is determined by the $\mathbf{d}\boldsymbol{p}$ coordinate of $a\eta_0$. Then as $a\neq 0$, $x_0\cdot\theta_0^{\perp}$ is determined by the $\mathbf{d}\boldsymbol{\theta}$ coordinate of $a\eta_0$, and finally $x_0\cdot\overline{\theta}_0=p$ determines x_0.

The assertion about H^s will be given because, although it is straightforward, it is not in the elementary literature. We prove one direction and leave the other to the reader. Let Rf be in $H^{s+1/2}$ near $(\theta_0,p_0;a\eta_0)$. Then, by Theorem 6.1 [24, p. 259], $Rf=u_1+u_2$ where $u_1\in H_c^{s+1/2}=H^{s+1/2}\cap\mathcal{E}'$, $u_2\in\mathcal{E}'$, and $(\theta_0,p_0;a\eta_0)\notin\text{WF}u_2$. Because R^{-1} is a Fourier integral operator continuous of order $\frac{1}{2}$ [8] and $u_1\in H_c^{s+1/2}$, $R^{-1}u_1\in H^s_{\text{loc}}(\mathbb{R}^2)$ [31]. R^{-1} is a Fourier integral operator associated to Γ (with $\mathbb{R}^2$ and $[0,2\pi]\times\mathbb{R}$ coordinates reversed) and so the "inverse" relation to (3.2) holds for R^{-1}. Therefore, as $(\theta_0,p_0;a\eta_0)\notin\text{WF}u_2$, $(x_0;a\overline{\theta}_0\mathbf{d}\boldsymbol{x})\notin\text{WF}\big(R^{-1}u_2\big)$. Therefore, $f=R^{-1}u_1+R^{-1}u_2$ is the sum of a distribution in H^s_{loc} and one that is smooth near $(x_0;a\overline{\theta}_0\mathbf{d}\boldsymbol{x})$. Therefore, by Theorem 6.1 [24, p. 259], f is microlocally H^s near $(x_0;a\overline{\theta}_0\mathbf{d}\boldsymbol{x})$. □

We now apply Theorem 3.1 and (3.3) to three common types of limited data tomography in the plane.

Example 3.3. *Limited angle tomography.* Let $U\subset[0,2\pi]$ be open, $U=U+\pi$ mod 2π. In limited angle tomography, one knows data $Rf(\theta,p)$ for all p and for $\theta\in U$. One can reconstruct $f(x)$ for all $x\in\mathbb{R}^2$ from limited angle data [21]. However, by (3.3), the only singularities of f that one can detect in a stable way are those with directions in U. To see this, choose $x\in\mathbb{R}^2$ and $\theta\in U$. Any wavefront of f at $(x;\overline{\theta}\mathbf{d}\boldsymbol{x})$ is detected by limited angle data because the line $\ell(\theta,x\cdot\overline{\theta})$ is in this data set. For the same reason, wavefront of f at $(x;\overline{\theta}\mathbf{d}\boldsymbol{x})$ for $\theta\notin U$ will not be stably detected by this limited angle data.

This phenomenon is illustrated by the singular functions in [14]. Those corresponding to large singular values (easy to reconstruct) oscillate generally in directions in U and those corresponding to small singular values (hard to reconstruct) oscillate generally in directions outside of U. This is also seen in the actual reconstructions from limited angle tomography.

Example 3.4. *The interior problem.* Let $M>1$ and assume supp $f\subset\{x\in\mathbb{R}^2\big||x|\leq M\}$. In this problem, one has data $Rf(\theta,p)$ for all θ but only for $|p|<1$. The goal is to reconstruct $f(x)$ for $|x|<1$. Simple examples show this is impossible in general. However, according to (3.3), one can detect all singularities of f in $|x|<1$. To see this, choose a point x inside the unit disk and choose a direction $\theta\in[0,2\pi]$. Then the line through x and normal to $\overline{\theta}$ is in the data set for interior tomography and so any singularity of f at $(x;\overline{\theta}\mathbf{d}\boldsymbol{x})$ is detected by interior data.

Lambda tomographic reconstructions are local—they use data $Rf(\theta,p)$ only for lines $\ell(\theta,p)$ near x to reconstruct at x. So Lambda tomography is useful for the interior problem. In fact, Lambda tomographic reconstructions for the interior problem clearly show the singularities of f in the unit disk [5]. Maass [18] has developed a singular value decomposition for this problem. See also [16].

Example 3.5. *The exterior problem.* Assume supp $f\subset\{x\in\mathbb{R}^2\big||x|\leq M\}$. Here one has data $Rf(\theta,p)$ for all θ but only for $|p|>1$. By [3] one can reconstruct $f(x)$ for $|x|>1$. Let $|x|>1$ and $\theta\in[0,2\pi]$. Then the only singularities of f at x that are reconstructed in a stable manner are those for θ with $\ell(\theta,x\cdot\overline{\theta})$ in the data set, that

is, for $|x \cdot \bar{\theta}| > 1$. Other singularities of f are not stably detected. This can be seen from the reconstructions in Figs. 1 and 2.

Lewitt and Bates [13], Louis [15], and Natterer [20] have developed good reconstruction algorithms that use exterior data. The author has developed an exterior reconstruction algorithm which employs Perry's singular value decomposition [23] and a priori information about the shape of the object to be reconstructed. Reconstructions for "medical" phantoms are in [26] and those for industrial phantoms are in [27], [28]. Exactly those singularities that are supposed to be stably reconstructed are clearly defined. In the author's algorithm, singularities that are not "visible" are smeared; reconstructions will now be given.

Figure 1 shows an object with outer radius $M = 1.5$ on a rectangular grid. The two bigger circles have density 1.5 and the two smaller 1.375. The annulus has density one. The reconstruction in Fig. 1b is gotten using the author's algorithm with noiseless data. The reconstruction in Fig. 1c is from the same algorithm but using data with slightly less than 1% L^∞ noise. Data are taken over lines using 100 values of p and 256 of θ [26]. In both reconstructions, the principle (3.3) is illustrated. However, the reconstruction with noise, Fig. 1c, shows some algorithm limitations as well (and reminds one that algorithm limitations independent of the principle can be important). The slightly darker areas in the background in Fig. 1c are the result of amplified high polar Fourier coefficients due to the noisy data.

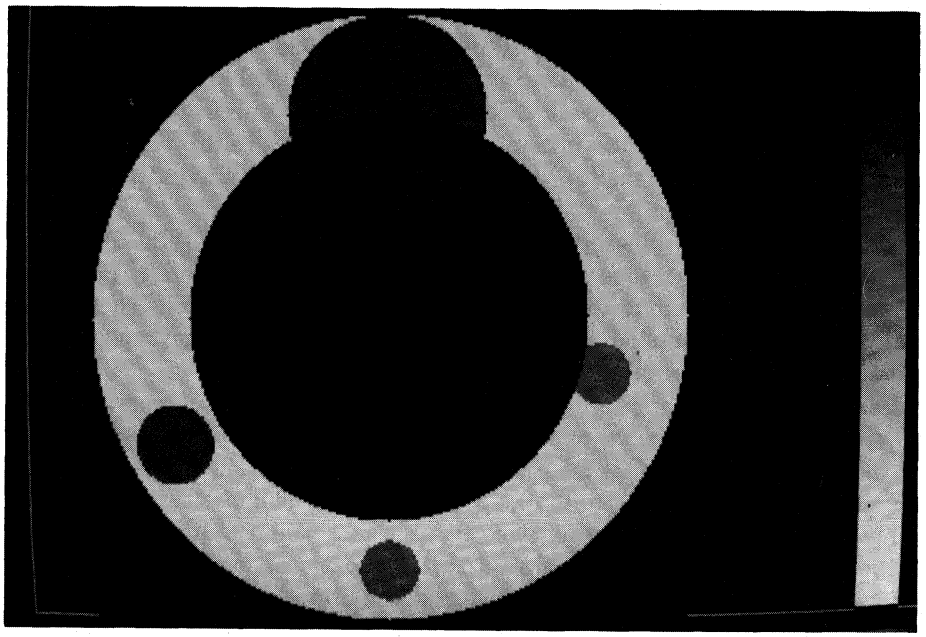

FIG. 1a. *Rectangular coordinate display of the phantom* [26] (*similar to the phantom in* [20]).

Figure 2 shows polar coordinate displays for $x = (r, \theta)$ with $\theta \in [\pi/8, 3\pi/8]$ on the horizontal axis and $r \in [1, 1.10]$ on the vertical axis ($r = 1.10$ at the bottom) [28]. To provide sufficiently fine radial resolution, the scale in r is magnified by a factor of 7.85. The phantom in Fig. 2 is supposed to represent a rocket motor with fuel of density 1.7 inside the circle of radius $r = 1.052$, an insulator of density 1.1 from

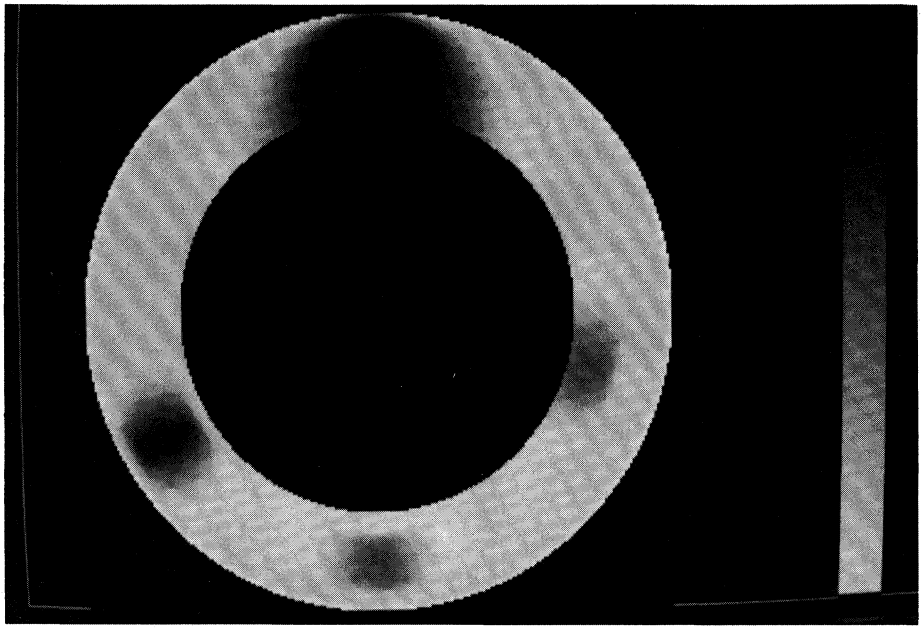

FIG. 1b. *Rectangular coordinate display of the reconstruction without noise of the phantom in Fig.* 1a [26].

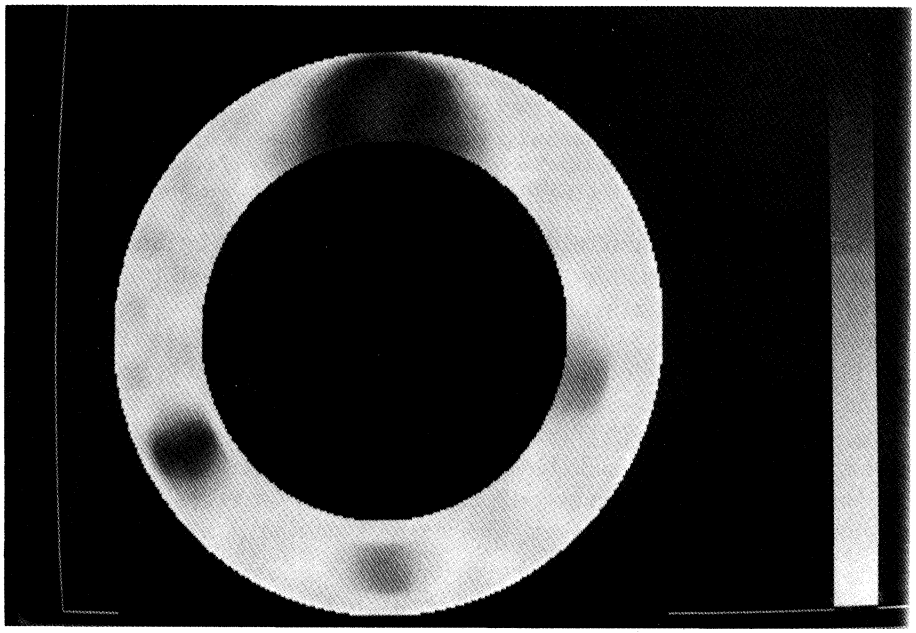

FIG. 1c. *Rectangular coordinate display of the reconstruction with noise of the phantom in Fig.* 1a [26].

$1.052 < r < 1.056$, and a shell of density 1.5 and outer radius $r = 1.093$. The defect rests against the inside boundary of the insulator and extends for 0.06 radians and is 0.0014 units thick (it is seen tangentially by only three detectors). It is centered at $\pi/4$ radians and has density zero. The reconstruction is done with 1% multiplicative L^∞ noise. Data are collected in a fan beam with 200 rays from $p = 1.0$ to $p = 1.10$ that emanate from the source in evenly spaced angles. The source and fan beam rotate around the object in 512 equally spaced angles.

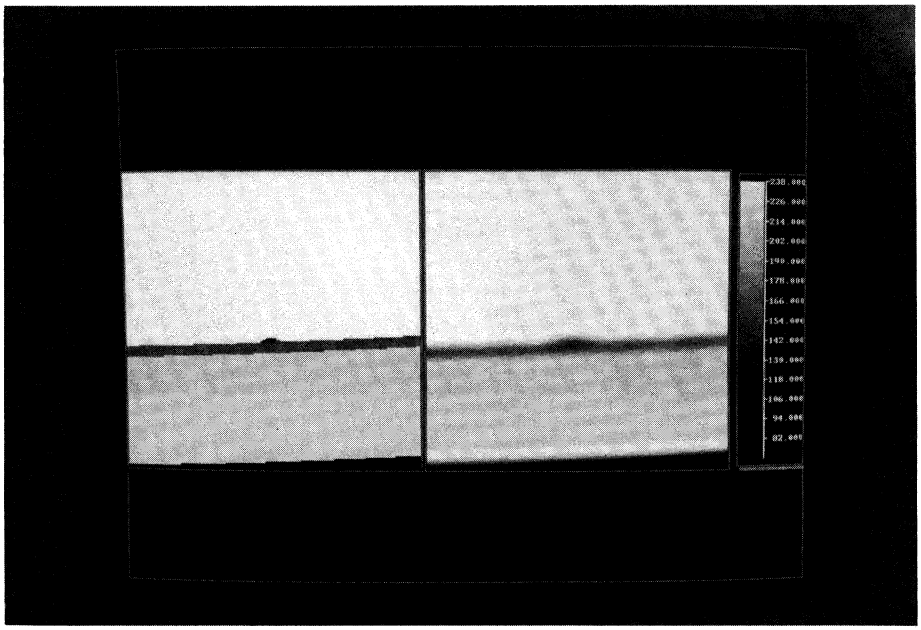

FIG. 2. *Polar coordinate display of rocket motor (phantom left, reconstruction with noise right)* [28]. *The "wedge" near* $r = 1.10$ *(at the bottom of the display) occurs because the center of the rocket is offset slightly from the center of the coordinate system.*

Because some wavefront directions are not stably detectable by limited angle data or by exterior data, inversion for these problems is highly ill-posed (see the example in [6] and the inverse discontinuity result in L^2 of [19]).

Reconstructions in Figs. 1 and 2 illustrate the principle (3.3). In the reconstruction in Fig. 1, the "sides" of the circles are blurred (corresponding to singularities normal to lines *not* in the data set), but the "inside" and "outside" boundaries of the circles are well reconstructed. This occurs despite the fact that only a few lines in the data set are tangent to the inside boundaries. The reconstructions of Fig. 2 are good (even though the problem is, in general, highly ill-posed) because all singularities are perpendicular to lines in the data set. This is true, even though the defect is very thin and short in extent.

4. The X-ray transform with sources on a curve in $\mathbb{R}^3$. The standard parameterization will be used for the divergent beam transform in $\mathbb{R}^3$. Let $\omega \in S^2$ and $x \in \mathbb{R}^3$, then the ray $\mathfrak{r}(\omega, x) = \{x + t\omega | t \geq 0\}$ is the ray parallel to ω and starting at x. The divergent beam transform of $f \in C_c(\mathbb{R}^3)$ is

$$Df(\omega, x) = \int_{t=0}^{\infty} f(x + t\omega)dt, \tag{4.1}$$

the integral of f over the ray $\mathfrak{r}(\omega, x)$. Typically, the sources for the divergent beam transform are points on a smooth closed curve γ. The divergent beam transform is defined for $f \in L^1_c(\mathbb{R}^3 \setminus \gamma)$ (L^1 functions of compact support in $\mathbb{R}^3 \setminus \gamma$) [9] (and even continuous on $\mathcal{E}'(\mathbb{R}^3 \setminus \gamma)$, [7]).

Inversion of the divergent beam transform is a limited data problem because data are given only over rays with sources on γ. Moreover, typically, X-rays are taken only over an open connected set, $\mathfrak{R}$, of rays with sources on γ. In general, as long as some ray in the data set is disjoint from supp f, then the part of f seen by the data (that is, supp $f \cap \left[\cup_{\mathfrak{r} \in \mathfrak{R}} \mathfrak{r}\right]$) is uniquely determined (see [9] and the generalization [2, Thm. 2.2]). Our theorem for the X-ray transform is as follows.

THEOREM 4.1. *Let γ be a smooth curve in $\mathbb{R}^3$ and $f \in \mathcal{E}'(\mathbb{R}^3 \setminus \gamma)$. Let $x_0 \in$ supp f and $\xi_0 \in T^*_{x_0}(\mathbb{R}^3) \setminus 0$. Then any wavefront set of f at $(x_0; \xi_0)$ is stably detected from data Df with sources on γ if and only if*

(4.2) *the plane $\mathcal{P}$, through x_0 conormal to ξ_0, intersects γ transversally.*

If data are taken over an open set of rays with sources on γ, then a ray in $\mathcal{P}$ from γ to x_0 must be in the data set for (4.2) *to apply. In these cases, f is in H^s microlocally near $(x_0; \xi_0)$ if and only if the corresponding singularity of Df is in $H^{s+1/2}$.*

The exact correspondence of singularities analogous to (3.2) can be obtained from the microlocal diagram (3.1.1) and the proof of Proposition 3.1.1 of [2]. Theorem 4.1 follows from [7] as well.

The global version of condition (4.2)—every plane meeting supp f intersects γ transversally—is called the Kirillov–Tuy condition. This condition is required for the inversion methods of Kirillov [12] and Tuy [32]. Under this condition, Finch [6] proves that $f \in H^s$ if $Df \in H^{s+1/2}$ for $s \geq \frac{1}{2}$ (and our theorem implies this fact for all s).

Typically, X-ray sources are placed on a circle surrounding the object to be reconstructed. Theorem 4.1 shows the singularities that are not detected by such data: singularities $(x_0; \xi_0)$ conormal to planes $\mathcal{P}$ not meeting the circle transversally. There are many such singularities—the more undetected singularities, the farther x_0 is from the plane of C. Finch [6] and others have noted that inversion with sources on one circle, C, is highly unstable. By analyzing the singular values, Maass shows that inversion is more stable for nonplanar curves such as two parallel circles or curves oscillating on a cylinder [17]. Condition (4.2) is another way to understand why inversion of data with sources on such nonplanar curves is better posed than for sources on one circle—in general, if the curve is nonplanar, more singularities can be detected stably from the given data.

Proof of Theorem 4.1. The microlocal assertion of Theorem 4.1 is a paraphrase of the comment about "type II complexes" below the statement of Proposition 3.1.1 of [2]. That comment is equivalent to the fact that if $x_0 \in \mathfrak{r}(\omega, y)$ for some $y \in \gamma$ and ξ_0 is conormal to ω then WFf at $(x_0; \xi_0)$ is detected by divergent beam data unless ξ_0 is conormal to γ at y. This is equivalent to condition (4.2). The statement about microlocal Sobolev spaces is valid because D is an elliptic Fourier integral operator of order $-\frac{1}{2}$ and so, if a singularity of f is detected by data Df, then the singularity of Df is $\frac{1}{2}$ order smoother than the corresponding singularity of f. This can be proven just as the analogous statement in Theorem 3.1 is proven. □

Acknowledgments. The author thanks Bar Ilan University and Universität des Saarlandes for their hospitality as this article was being written. He is indebted to A. Zaslavsky for lively and informative conversations about his article with A. G.

Ramm [29]. He is also indebted to the many conversations with Adel Faridani, Alfred Louis, Peter Maass, Frank Natterer, Kennan Smith, and others over the years that have helped develop and refine the ideas in this article. Finally, the author thanks the Institut für Numerische und instrumentelle Mathematik der Universität Münster for the display programs for Fig. 2.

REFERENCES

[1] M. D. ALTSCHULER, *Reconstruction of the global-scale three-dimensional solar corona*, in Image Reconstruction From Projections, Implementation And Applications, G. T. Herman, ed., Topics Appl. Phys., 32, Springer-Verlag, New York, Berlin, pp. 105–145.

[2] J. BOMAN AND E. T. QUINTO, *Support theorems for real-analytic Radon transforms on line complexes in three-space*, Trans. Amer. Math. Soc., 335 (1993), pp. 877–890.

[3] A. M. CORMACK, *Representation of a function by its line integrals with some radiological applications*, J. Appl. Phys., 34 (1963), pp. 2722–2727.

[4] M. DAVISON, *The ill-conditioned nature of the limited angle tomography problem*, SIAM J. Appl. Math., 43 (1983), pp. 428–448.

[5] A. FARIDANI, E. L. RITMAN, AND K. T. SMITH, *Local tomography*, SIAM J. Appl. Math., 52 (1992), pp. 459–484.

[6] D. V. FINCH, *Cone beam reconstruction with sources on a curve*, SIAM J. Appl. Math., 45 (1985), pp. 665–673.

[7] A. GREENLEAF AND G. UHLMANN, *Non-local inversion formulas in integral geometry*, Duke J. Math., 58 (1989), pp. 205–240.

[8] V. GUILLEMIN AND S. STERNBERG, *Geometric Asymptotics*, Amer. Math. Soc., Providence, RI, 1977.

[9] C. HAMAKER, K. T. SMITH, D. C. SOLMON, AND S. L. WAGNER, *The divergent beam X-ray transform*, Rocky Mountain J. Math., 10 (1980), pp. 253–283.

[10] L. HÖRMANDER, *Fourier integral operators* I, Acta Math. 127 (1971), pp. 79–183.

[11] ———, *The Analysis of Linear Partial Differential Operators* I, Springer-Verlag, New York, 1983.

[12] A. A. KIRILLOV, *On a problem of I. M. Gel'fand*, Soviet Math. Dokl., 2 (1961), pp. 268–269.

[13] R. M. LEWITT AND R. H. T. BATES, *Image reconstruction from projections*. II: *Projection completion methods (theory)*, Optik, 50 (1978), pp. 189–204; III: *Projection completion methods (computational examples)*, Optik, 50 (1978), pp. 269–278.

[14] A. LOUIS, *Incomplete data problems in X-ray computerized tomography* 1. *Singular value decomposition of the limited angle transform*, Numer. Math., 48 (1986), pp. 251–262.

[15] ———, private communication.

[16] A. LOUIS AND A. RIEDER, *Incomplete data problems in X-ray computerized tomography* II. *Truncated projections and region-of-interest tomography*, Numer. Math., 56 (1989), pp. 371–383.

[17] P. MAASS, 3D *Röntgentomographie: Ein Auswahlkriterium für Abtastkurven*, Z. Angew. Math. Mech., 68 (1988), pp. T498–T499.

[18] ———, *The interior Radon transform*, SIAM J. Appl. Math., 52 (1992), pp. 710–724.

[19] W. MADYCH AND S. NELSON, *Reconstruction from restricted Radon transform data: resolution and ill-conditionedness*, SIAM J. Math. Anal., 17 (1986), pp. 1447–1453.

[20] F. NATTERER, *Efficient implementation of "optimal" algorithms in computerized tomography*, Math. Meth. Appl. Sci., 2 (1980), pp. 545–555.

[21] ———, *The mathematics of computerized tomography*, John Wiley, New York, 1986.

[22] V. PALAMODOV, *Nonlinear artifacts in tomography*, Sov. Phys. Dokl. 31 (1986), pp. 888–890.

[23] R. M. PERRY, *On reconstruction of a function on the exterior of a disc from its Radon transform*, J. Math. Anal. Appl., 59 (1977), pp. 324–341.

[24] B. PETERSEN, *Introduction to the Fourier Transform and Pseudo-Differential Operators*, Pittman, Boston, 1983.

[25] E. T. QUINTO, *The dependence of the generalized Radon transform on defining measures*, Trans. Amer. Math. Soc. 257 (1980), pp. 331–346.

[26] E. T. QUINTO, *Tomographic reconstructions from incomplete data–numerical inversion of the exterior Radon transform.*, Inverse Problems, 4 (1988), pp. 867–876.

[27] ———, *Limited data tomography in non-destructive evaluation*, Signal Processing Part II: Control Theory And Applications, IMA Vol. Math. Appl., 23, Springer-Verlag, New York, 1990, pp. 347–354.

[28] ———, *Computed tomography and Rockets*, in Mathematical Methods In Tomography, Proceedings, Oberwolfach, 1990, Lecture Notes in Math., 1497, Springer-Verlag, Berlin, New York, 1991, pp. 261–268.

[29] A. G. RAMM AND A. I. ZASLAVSKY, *Reconstructing singularities of a function from its Radon transform*, preprint.

[30] L. A. SHEPP AND S. SRIVASTAVA, *Computed tomography of PKM and AKM exit cones*, AT & T. Tech. J., 65 (1986), pp. 78–88.

[31] F. TREVES, *Introduction to Pseudodifferential and Fourier integral operators* II, Plenum Press, New York, 1980.

[32] H. K. TUY, *An inversion formula for cone-beam reconstruction*, SIAM J. Appl. Math., 43 (1983), pp. 546–552.